Soft Matter

COMMUNICATION

View Article Online
View Journal | View Issue

Cite this: *Soft Matter*, 2022, **18**, 8554

Received 27th July 2022,
Accepted 29th October 2022

DOI: 10.1039/d2sm01013e

rsc.li/soft-matter-journal

Cellular micromasonry: biofabrication with single cell precision†

S. Tori Ellison,[a] Senthilkumar Duraivel,[a] Vignesh Subramaniam,[b] Fredrik Hugosson,[c] Bo Yu,[d] Joseph J. Lebowitz,[e] Habibeh Khoshbouei,[e] Tanmay P. Lele,[fgh] Mark Q. Martindale[c] and Thomas E. Angelini *[abi]

In many tissues, cell type varies over single-cell length-scales, creating detailed heterogeneities fundamental to physiological function. To gain understanding of the relationship between tissue function and detailed structure, and eventually to engineer structurally and physiologically accurate tissues, we need the ability to assemble 3D cellular structures having the level of detail found in living tissue. Here we introduce a method of 3D cell assembly having a level of precision finer than the single-cell scale. With this method we create detailed cellular patterns, demonstrating that cell type can be varied over the single-cell scale and showing function after their assembly.

Introduction

The different cell types that constitute living tissue are often structured into highly heterogeneous and complex spatial patterns; cell type can differ over length-scales as small as a single cell within a given tissue.[1,2] This spatial heterogeneity is broadly linked to different types of tissue function. For example, to maintain high rates of molecular exchange in the liver, a network of endothelial cells, called the sinusoid, permeates the periportal zone where every hepatocyte is located within one or two cell diameters of an endothelial capillary.[3,4] Another dramatic example is found in the pancreatic islet, where the five main cell types of the islet are located within a few cell diameters of one another, making frequent contacts with acinar and ductal cells of the exocrine pancreas.[5–7] This highly heterogeneous arrangement of cell types within the islet's relatively small volume allows cells to communicate through secretion and maintain blood glucose homeostasis.[5–7] The connection between small-scale structural heterogeneity and tissue function is also exhibited by glandular acini *in vitro*.[8–10] These hollow spheres are made from epithelial monolayers surrounded by a basement membrane; the signaling between the basement membrane and cell nuclei is crucial for acini to develop and function.[8,11–14] While glandular acini represent an *in vitro* system in which the link between tissue structure and function can be studied in detail, it remains exceedingly challenging to reproduce the complex cellular patterns found more generally *in vivo*. For example, relying on spontaneous or guided processes of multi-cellular self-assembly within bioengineered tissues is time consuming and does not precisely reproduce the detailed structural and functional heterogeneity at the single-cell scale found within *in vivo* tissues.[15–17] 3D bioprinting provides control and repeatability for structuring *in vitro* tissue models, but current tools are not sufficiently precise to produce spatial variations in cell type over the scale of even a few cells, much less a single cell.[18] Trying to achieve single cell resolution by extrusion-based bioprinting through a narrow cell-sized nozzle risks persistent clogging and damage to the cells from shear stresses. Thus, to create tissue models that reproduce the spatial heterogeneities found within *in vivo* tissue, new biofabrication tools with single-cell precision are needed. Without such tools, our basic understanding of how tissue function collectively emerges from spatially heterogeneous tissue structure will continue to depend on observations and methods that rely dominantly on cell-directed organization, which have persistently challenged researchers.

[a] *Department of Material Sciences and Engineering, University of Florida, Gainesville, Florida 32611, USA. E-mail: t.e.angelini@ufl.edu*
[b] *Department of Mechanical and Aerospace Engineering, University of Florida, Gainesville, Florida 32611, USA*
[c] *The Whitney Laboratory for Marine Bioscience, St. Augustine, Florida 32080, USA*
[d] *Department of Chemical Engineering, University of Florida, Gainesville, Florida 32611, USA*
[e] *Department of Neuroscience, University of Florida, Gainesville, Florida 32611, USA*
[f] *Department of Biomedical Engineering, Texas A&M University, College Station, Texas 77843, USA*
[g] *Artie McFerrin Department of Chemical Engineering, Texas A&M University, College Station, Texas 77843, USA*
[h] *Department of Translational Medical Sciences, Texas A&M University, Houston, Texas 77843, USA*
[i] *J. Crayton Pruitt Family Department of Biomedical Engineering, University of Florida, Gainesville, Florida 32611, USA*

† Electronic supplementary information (ESI) available: Fig. S1–S4, Movies S1–S3, Methods and materials. See DOI: https://doi.org/10.1039/d2sm01013e

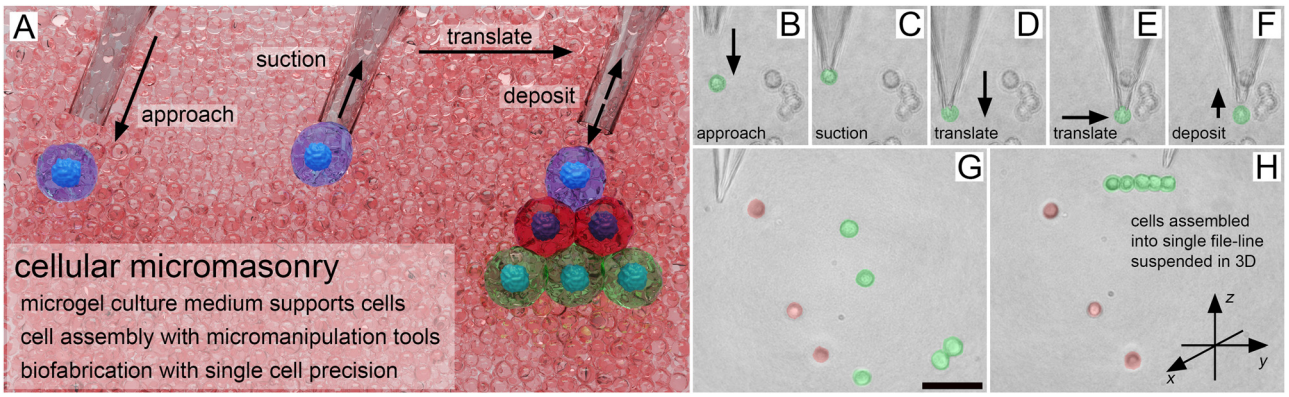

Fig. 1 (A) With the micromasonry technique, cellular structures are precisely assembled in 3D space within a microgel-based culture medium that provides stabilizing support. Dispersed cells are retrieved, translated, and deposited using a micromanipulator equipped with a glass microcapillary connected to a suction generator, all mounted on a confocal microscope. Shown here, a 3t3 fibroblast cell suspended in 3D is (B) approached and (C) retrieved by applying a light suction. (D and E) The cell is translated to a chosen location in 3D space and (F) deposited. (G) Cells are dispersed in 3D; green cells are selected for assembly, while red cells are left in place (3t3 fibroblasts, false colouring. Scale bar: 30 μm; applies to panels (B–H)). (H) The green cells are picked up, translated, and placed next to each other forming a single-file line of cells, suspended in 3D space.

In this brief communication we introduce a method that enables us to emulate the heterogeneous spatial patterning found *in vivo* with single-cell precision. The method, which we call "cellular micromasonry", combines a soft 3D support medium with micromanipulation and 3D microscopy. The 3D support medium is a phase of soft matter made from jammed granular-scale microgels – hydrogel microparticles packed together that form the microscopic equivalent of the "ball pit" children play in.[19–21] Children in ball pits can lay still, supported by the static forces of the packed balls, yet they can also swim through the balls, embedding themselves deep within their surroundings. By analogy, here we use micromanipulators to grasp, translate, and place cells in a "ball pit" made from microscopic hydrogel particles swollen in liquid cell growth media (Fig. 1A). This microgel medium is strong enough to support the cellular structures, but weak enough that a microcapillary holding cells can easily be translated through it; the microgels' low polymer concentration limits the physical stress on cells as we build with them.[19–22] We use this method to methodically place cells in precisely structured patterns, controllably alternating between different cells, one-by-one. With this approach, we demonstrate that single-cell precision in spatial heterogeneity can be achieved with a biofabrication tool. To test for function, we study molecular transport through gap junctions, observing calcein dye diffusing from cell-to-cell, and we show that glandular acini can develop within this medium. The cellular micromasonry method enables the building of stratified, precise cellular structures for detailed investigations of the relationship between structure and function in models of both developing and mature tissues.

Results

To create precise cellular structures, we formulate a microgel support medium in which the microgels are approximately 4 μm in diameter. We require microgels larger than 1 μm in diameter to suppress their thermally driven translocation. At the same time, we require microgels smaller than the size of a cell since we want the ability to place cells with sub-cellular spatial precision and the microgel size sets the size-scale of this limit; microgels must rearrange at least locally to accommodate cell translation. We harvest cells from their traditional culture conditions and manually disperse them with a pipette into this microgel culture medium contained in a glass-bottomed Petri dish (see Methods, ESI† for cell types and culture details). The dish is mounted onto a temperature-controlled stage atop an inverted confocal microscope. When using carbonate-based culture buffers, humidified CO_2 is gently blown onto the sample surface to maintain neutral pH in the microgel culture medium. Using the microscope, we identify a chosen cell, translate the tip of a microcapillary to its surface using the micromanipulator, and lightly aspirate using a CellTram (Eppendorf), applying suction. Once the cell is captured, it is translated to the desired location and deposited (Movie S1, ESI†). By repeatedly capturing, translating, and depositing cells, we assemble structures suspended in 3D space without having to build up from a solid support (Fig. 1B–F).

To provide support to cells while minimizing the shear stress they endure as we build structures, ensuring the cells are gently cradled in their 3D microenvironment, we optimized the microgel medium through rheological testing. We find that microgel media formulated at 5–6% (w/w) polymer has an elastic shear modulus of 10–20 Pa and a yield stress of 1.3–2.4 Pa (see Fig. S1 and Methods, ESI† for microgel polymer species). This level of shear stress is comparable to fluid stresses frequently imposed on cell surfaces, so we do not expect this procedure to lead to cell damage.[23] As the microcapillary translates back and forth throughout the micromasonry process of building structures, the microgel "balls" are forced to rearrange and flow around the microcapillary surface. To determine whether these rearrangements lead to

irreversible, long-ranged, or erratic flow patterns in the microgel medium, we performed video imaging of a microcapillary translating through the microgel medium containing dispersed cells, moving at approximately 0.5 mm s^{-1}, which is the rate we translate the microcapillary during micromasonry procedures (Movie S2, ESI†). We find that when the microcapillary is reciprocally translated near suspended cells, the net cell displacement is approximately one cell diameter or less; cells further from the capillary exhibit less hysteresis than cells directly in the path of the microcapillary (Fig. S2, ESI†).

Analysis of the microgel flow-field around the translating microcapillary helps to explain this reversibility in microgel displacement during the micromasonry process (Fig. S3, ESI†). To understand this apparent hydrodynamic reversibility with the micromasonry method, we estimate the Reynolds' number, Re, given by $\rho v d/\eta$, where ρ is the microgel mass density, v and d are the microcapillary translation speed and diameter, respectively, and η is the medium viscosity.[24] The microcapillary diameter, d, is 1 mm along its shaft and approximately 5 μm near its tip, so we approximate the shear-rate range to be $v/d \approx 0.5$–100 s^{-1}. The corresponding microgel viscosity range from rheological measurements is 0.2–10 Pa s (Fig. S1C, ESI†). Thus, we estimate the maximum Re occurring during micromasonry to be approximately 10^{-3}, four orders of magnitude below the flow regime where hydrodynamic reversibility begins to break down.[25] Consequently, the predictable flow behavior of the packed microgel medium enables the assembly of precise structures in 3D space, like single-file lines of cells (Fig. 1G and H). We use such single-file line structures to quantify the precision of the micromasonry method, measuring the standard deviation, σ, of cell position relative to the centerline. We find σ = 1.6 μm (averaged across N = 3 different samples), many times smaller than the mean cell diameter of 18.8 ± 2.7 μm (mean ± standard deviation). Even the 99.7% confidence interval of 6σ is half the mean cell size, consistent with sub-cellular precision in cell positioning. These errors could arise from a variety of sources including the polydispersity of the microgel particles or the irreversible component of the displacement field around the translating microcapillary tip during cell positioning steps.

The heterogeneous composition of tissues *in vivo* often exhibit cell-type variations over length-scales as small as the individual cell; to mimic this extreme variability *in vitro*, we build structures from cells labeled with different fluorescent dyes. Two populations of Madin-Darby Canine Kidney (MDCK) cells are cultured under standard 2D conditions, labeling one population with CellMask orange and the other with 5-chloromethylfluorescein diacetate (CMFDA). To create a source population of cells to build with, the cells are harvested and suspended in a glass-bottom Petri dish filled with 2 mL of the microgel culture medium. The dish is placed on an inverted confocal microscope equipped with an incubating plate, keeping the cells at 37 C (Fig. 2A). To test our ability to generate a diversity of spatial patterns that may occur in different tissues, we assembled several basic structures: a line of alternating colors, a triangle with rows of alternating color, a six-fold packing of red cells around a central green cell, and the unit cell of a honeycomb lattice (Fig. 2B). We envision using micromasonry to study the emergence of collective behavior as a function of tissue size. To demonstrate this capability, we built different sized structures of a repeating checkerboard pattern (Fig. 2C). While some highly ordered tissues exhibit regular patterns like those shown here, even these highly ordered structures often lay on curved manifolds in space. For example, the organ of Corti exhibits highly ordered checkerboard patterning and hexagonal packing over the curved surface of the cochlear duct.[26] Thus, to explore the possibility of using micromasonry to build larger objects with larger-scale structural complexity than simple geometric shapes, we constructed the initials of our institution, 'UF' out of almost 100 cells, suspended in 3D space (Fig. 2E). Taken together, these tests of patterning at the single-cell scale and complex structuring at the large-scale demonstrate the potential for using micromasonry to mimic the complexity of *in vivo* tissues.

To determine if the cells in these fabricated structures are functionally interacting with one another, we use a calcein dye

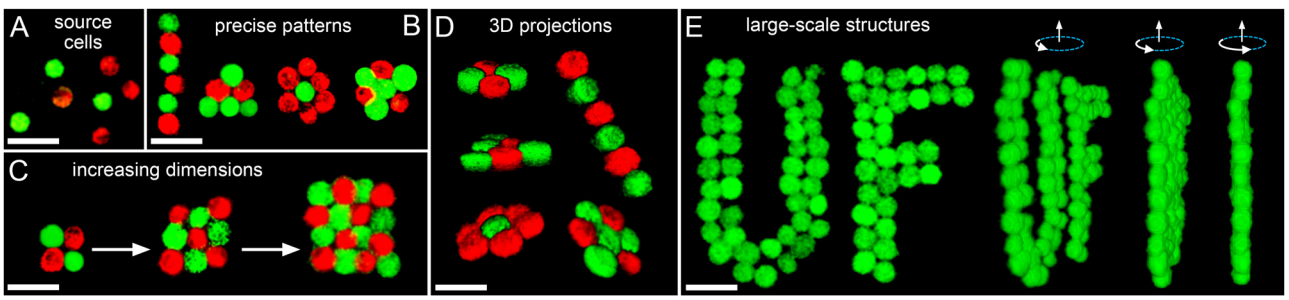

Fig. 2 MDCK cell populations are assembled into precise structures. (A) Red and green cells are dispersed randomly in the microgel medium. (scale bar: 50 μm) (B) Cells are retrieved and assembled into patterns with single cell precision, like the single-file line with alternating cell colors. While hexagonal packing is expected for spheres, with micro-masonry such structures can be made with different patterning. (scale bar: 50 μm) (C) Square packings are possible and the emergence of collective behaviour can be studied by increasing the dimensions of a given pattern. (scale bar: 50 μm) (D) The small-scale patterns are shown from different angles to demonstrate control over cell placement in the third dimension. The cells are seen to be co-planar, suspended in 3D space. (scale bar: 30 μm) (E) Single cells are arranged into large irregular shapes of specific design, such as the initials of the authors' institution. Viewed from different angles, we see cell placement along the third dimension is extremely precise. (scale bar: 50 μm).

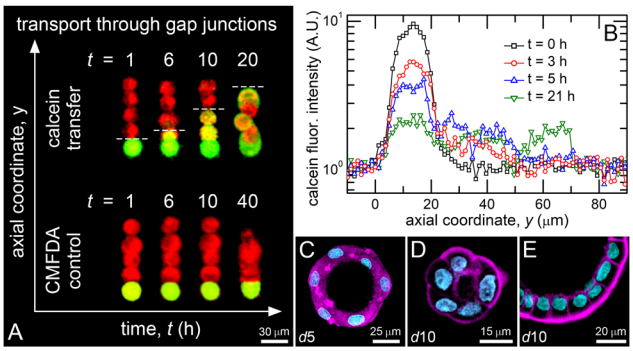

Fig. 3 Functional assays. (A) As a functional test, we perform a calcein transport assay. Four red cells are assembled in a line and one cell dyed with calcein is placed on the end (top). All the cells become fluorescent green over 20 hours, indicating that gap junctions form, allowing the calcein dye to travel from cell to cell. In control experiments, a cell dyed with CMFDA is placed on the end of the red-cell line; CMFDA is gap-junction impermeable (bottom). We see no CMFDA transport in these experiments. (B) Space-time analysis of calcein fluorescence intensity shows the calcein transferring from the source cell to the neighboring cells. (C–E) As a second functional assay we study acini formation in the microgel medium. (C) After five days we see hollow shells forming with disordered cytoskeletal structure. (D and E) After 10 days we see structures resembling mature acini (cyan: Hoescht; magenta: Alexa-phalloidin) images of larger whole acini can be found in Fig. S4 (ESI†).

assay to test whether gap junctions form. Gap junctions are plaques of intercellular nano-channels that form between neighbouring cells that allow the diffusion of small molecules from cell to cell. This transport can be visualized using calcein acetoxymethyl (AM) ester (calcein AM), a cell-permeant live cell dye.[27] In live cells, calcein AM is converted to freely diffusing green fluorescent calcein through acetoxymethyl ester hydrolysis, intracellularly. When gap junctions are present, calcein dye can be observed passing from cell to cell with fluorescence microscopy.[27] We culture MDCK cells in 2D, dye separate populations with CellMask orange and calcein AM, harvest the cells, and randomly disperse both populations as described above. Using the micromasonry technique, we build single-file lines of four red cells and then add a single green cell to the end of the line (Fig. 3A). A confocal Z-stack is taken every 30 minutes for 24 hours. Throughout this period of time we see the green dye travel down the line of cells, indicating that gap junctions indeed form in these manufactured cellular structures (Fig. 3B). We find that the calcein dye takes about 5 hours to travel from cell to cell, which agrees with results from standard calcein assays.[27] To ensure this observation requires gap junction permeable dyes, we perform control experiments in which CMFDA is used in place of calcein; CMFDA cannot pass through gap junctions. In these control experiments, the green dye does not spread from cell to cell (Fig. 3A). These results demonstrate that structures suspended in the 3D microgel medium and assembled with the micromasonry technique maintain their capacity to form the functional gap junctions typically observed in more traditional culture contexts.

As a second functional assay, we test whether glandular acini can form within microgel media. Acini represent one of the best established and widely used tissue models; acini formed from mammary epithelial cells are used in breast cancer research, for example.[8–11] Paralleling standard protocols, we disperse MDCK cells into a modified microgel media that is swollen in diluted Matrigel (see Methods, ESI†). After about 10 days of incubation, we see that single cells have proliferated and self-assembled into the monolayer shell structures characteristic of traditionally cultured acini. To compare the architecture of these epithelial shells to traditional acini, we fix and stain them with Hoeschst 33342 and Alexa 594 phalloidin to visualize the nucleus and actin cytoskeleton. We image the stained tissues with confocal microscopy where we see the characteristic monolayer shell structure as well as the polarized cytoskeletal structure typically found in acini (Fig. 3C–E and Fig. S4, ESI†). Slices through the 3D confocal stacks exhibit actin assembly near the outer-facing surface of the shell where a basement membrane is known to form.[8–11] These results represent a new way to culture glandular acini and point toward a future path of rich exploration; the cells' mechanical microenvironment can be tuned by preparing the microgels at different concentrations, and the granular nature of the microgel medium allows for the micromasonry technique to be combined with spontaneous acini formation. For example, different cell types can be delivered to the maturing acini at chosen locations and times, or concentrated doses of growth factors or other stimulatory molecules can be locally perfused with the micromasonry instrument. Such a hybrid approach could be used to expand the experimental toolbox for broader investigation of diverse tissue models of healthy development or disease processes.[28–30]

To take the first steps toward using micromasonry for studying more complex cellular structures and potentially manipulating their function, we pack pluripotent embryonic cells around a functionalized microsphere. Following established protocols, blastula stage embryos (24 h post fertilization) from the starlet sea anemone, *Nematostella vectensis*, injected with mRNA for green fluorescent protein as zygotes, are dissociated into single cells in calcium and magnesium free sea water. The dissociated cells are manually collected with a micropipette and dispersed in the microgel medium. Since these embryos are cultured in sea water, we developed a zwitterionic microgel formulation that does not de-swell at high salt concentrations (see Methods, ESI†). We first built several simple planar structures from the dissociated cells (Fig. 4A). We then dispersed fibronectin-coated polystyrene microspheres in the microgel medium and built a hybrid biotic/abiotic structure in which the dissociated embryonic cells were deposited on the bead's surface (Fig. 4B). Time-lapse microscopy revealed the cells remained viable and motile, actively spreading on the bead over the course of 13 h (Movie S3, ESI†). While we need to further study how these cells respond to a process of disassembly and re-assembly on a foreign surface, this demonstration of hybrid biotic/abiotic assembly is key to developing advanced biomaterials that precisely combine living cells with engineered microstructures.[31]

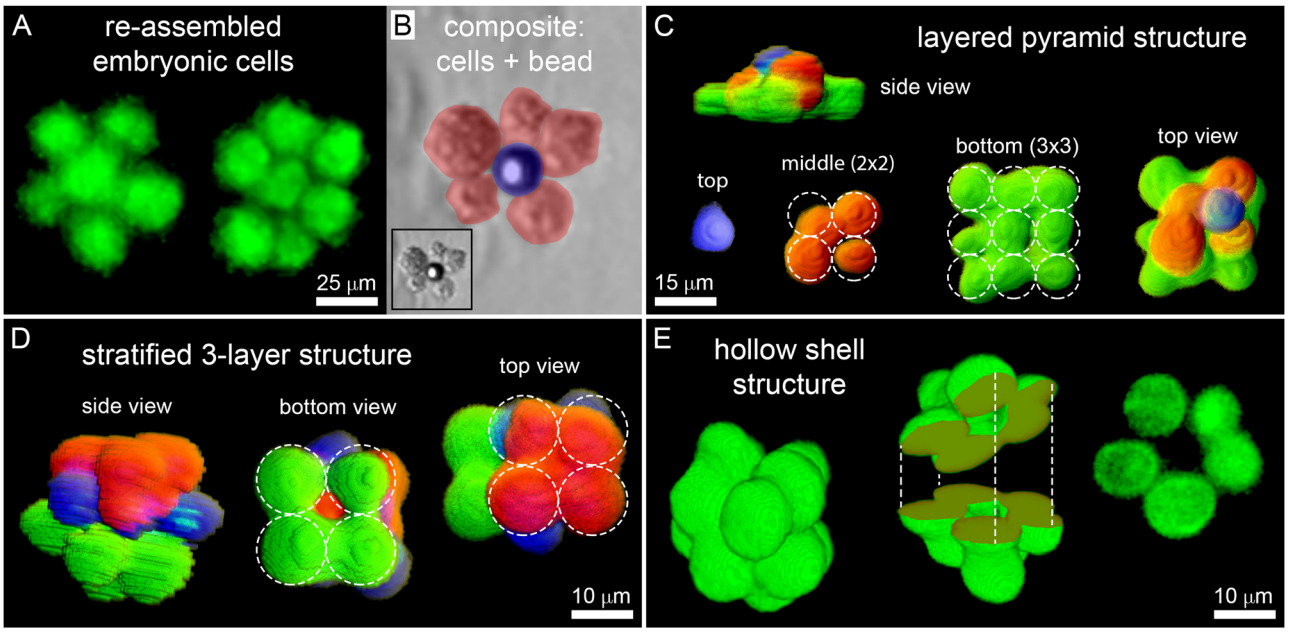

Fig. 4 (A) Fluorescently labeled cells (GFP) from the sea anemone *Nematostella vectensis* embryos are disassociated, dispersed in the microgel medium, and used to build planar structures. (B) The embryonic cells are placed around a fibronectin-coated bead to observe their interactions with an anchoring surface in 3D (false colored; inset: uncoloured bright-field image). (C) MDCK cells are dyed blue, red, and green to create three different populations. Three-color, 3D structures are assembled including a layered pyramid and (D) a stratified three layer structure (dashed circles indicate perfect assembly). (E) A hollow spherical structure is built from MDCK cells dyed with CMFDA mimicking the structure of acini (left and center: volume-view renderings; right: *X*–*Y* slice).

To test for the potential of using micromasonry to build layered 3D structures having heterogeneities over length-scales of single cells, approximating the level of detail found in dense living tissues, we build a series of stratified objects from three separate cell populations. Extending the methods described above, we label MDCK cells with blue, green, and red dyes and selectively retrieve chosen cells from a randomly dispersed population to build layered patterns. We create a square pyramid structure by assembling a planar 3×3 square packing of green cells, followed by a 2×2 layer of red cells, finishing with a single blue cell at the apex (Fig. 4C). Similarly, we build a stack of 2×2 layers, with green cells forming the base, blue cells forming the middle layer, and red cells on top (Fig. 4D). Although there are imperfections in both structures, no imperfection is more than a single cell diameter, indicating that extremely precise, multicellular structures can be built using this method. As a final test of the potential for using micromasonry to build tissue models, we assemble a spherical shell of MDCK cells to approximate a glandular acinus. 3D renderings of this assembly reveal its shell structure; slices through the 3D structure show the open pore-space inside the shell of cells (Fig. 4E). While these structures were imaged immediately after building, our functional assays of MDCK structures showing gap junction formation and the development of characteristic acini structure over time indicate that these more complex 3D structures may evolve into functional tissue models (Fig. 3). We envision that the combination of micromasonry and optimal culture conditions will facilitate building "acini on demand" where the rapid integration of structural and microenvironmental cues could accelerate the development of mature acini, with the possibility of extending this principle to other tissue models.

Conclusions

All the cellular structures shown here were assembled by operating the micromasonry system by hand, in which a researcher dispersed cells into the microgel medium with a pipette, identified individual cells by eye on a microscope, and meticulously assembled them into the targeted designs by turning dials on micromanipulator control hardware. While single-cell precision was achieved with this manual approach, the current procedure limits the physical scale of structures that can be assembled. However, we believe that all the steps in cellular micromasonry can be automated by combining a diversity of current engineering tools like 3D image segmentation, 3D cell tracking, and the control algorithms of pick-and-place robotics.[32] Indeed, comparable approaches have been used to assist in colloidal assembly with optical trapping methods.[33–35] Imaging deep into even modestly sized 3D structures to guide the micromasonry process may require advanced imaging techniques like multi-photon microscopy to increase light penetration, or adaptive optical confocal fluorescence microscopy to reduce the effects of optical abberations.[36,37]

Micropipette-based tools have been used for the assembly and fusion of tissue aggregates, spheroids, and micro-patterned cellular assemblies, though the challenges of automated building

with single cells may require different strategies.[38–43] For example, since building within the microgel medium creates uncertainties like elastic and plastic material deformations on the scale of the single-cell building-blocks themselves, we believe new computational tools based on machine learning and artificial intelligence for controlling machine operations in uncertain environments can be employed as a path forward to rapidly build larger and more complex structures with an even higher level of precision than that demonstrated here.[32] If these approaches eliminated the incidence of significant positioning errors, then we expect that large structures could be assembled over short times. For example, at current translation speeds of 0.5 mm s^{-1}, if each cell was moved by 1 mm, accounting for the return trip and allowing for approximately 1 second to apply or release suction, the rate of cell deposition is 4 s per cell. Thus structures made from 900 cells could be built in one hour. A skilled researcher couple potentially assemble 100 cells in an hour, manually, allowing for a 10-fold decrease in efficiency in capturing and positioning each cell.

As improved micromasonry tools are developed for creating larger-scale structures, smaller-scale manual micromasonry can now be used to explore the structure-function relationship in model tissues. Cell-to-cell signalling occurs extensively throughout embryonic development, with cell fate and behaviour responding to embryonic ''organizing centres''. In some embryos this function is performed by a single cell that establishes the fate of all surrounding cells.[44] By dissociating developing embryos and using the micromasonry technique to deliver the organizing cell to different complements of surrounding ''responding'' cells, the sensitivity of cell signalling to cell positioning in these processes can be quantitatively investigated. Such an approach could be broadened by leveraging our ability to easily manipulate gene expression in model developmental systems like *Nematostella*.[44,45] Similarly, a hybrid approach to organoid engineering could be developed. A dominating paradigm in organoid research is to program successive stages of differentiation into pluripotent cells that will spontaneously and collectively mature into functioning differentiated cellular structures that approximate mature organ behavior.[45,46] By building pre-structured assemblies from pluripotent cells and delivering additional programmed cells at precisely chosen locations at critical time-points, the organoid maturation process could be rapidly and controllably guided down many steps of differentiation and development. Finally, with the ability to create cellular structures having crystalline symmetry and spacing, as shown in Fig. 2, combined with the cell programming tools of synthetic biology, cell–cell signalling could be synchronized with a level of coherence and function that does not emerge from random cell patterns.[45–47] While current trends in 3D bioprinting research largely focus on fabricating large-scale functional engineered tissues, we hope the cellular micromasonry technique introduced in this brief communication inspires researchers to also work in the opposite direction, using the methods, materials, and tools of biofabrication to conduct fundamental investigations of collective cell behaviour at a level of structural detail approaching that found *in vivo*.

Conflicts of interest

There are no conflicts to declare.

Acknowledgements

The authors would like to thank Anton Paar for use of their rheometer through the Anton Paar VIP research program. This research was supported by the University of Florida Foundation project #T17581.

Notes and references

1 S. A. Newman, G. Forgacs and G. B. Muller, *Int. J. Dv. Biol.*, 2006, **50**, 289–299.
2 L. Wolpert, *Developmental Biology: A Very Short Introduction*, 2011.
3 T. Kietzmann, *Redox*, 2017, **11**, 622–630.
4 K. K. Sorensen, J. Simon-Santamaria, R. S. McCuskey and B. Smedsrod, *Compr Physiol.*, 2015, **5**, 1751–1774.
5 J. Li, J. Klughammer, M. Farlik, T. Penz, A. Spittler, C. Barbieux, E. Berishvili, C. Bock and S. Kubicek, *EMBO Rep.*, 2016, **17**, 178–187.
6 S. Speier, *et al.*, *Nat. Med.*, 2008, **14**, 574–578.
7 K. Aamodt and A. Powers, *Diabetes, Obes. Metab.*, 2017, **19**, 124–136.
8 P. A. Kenny, *et al.*, *Mol. Oncol.*, 2007, **1**(1), 84–96.
9 M. J. Bissell and D. Radisky, *Nat. Rev. Cancer*, 2001, **1**(1), 46–54.
10 L. E. O'Brien, M. M. Zegers and K. E. Mostov, *Nat. Rev. Mol. Cell Biol.*, 2002, **3**, 531–537.
11 J. Debnath, *et al.*, *Science Direct*, 2003, **30**(3), 256–258.
12 G. Y. Lee, *et al.*, *Nat. Methods*, 2007, **4**, 359–365.
13 K. L. Schmeichel and M. J. Bissell, *J. Cell Sci.*, 2003, **15**(116), 2377–2388.
14 D. E. Discher, P. Janmey and Y. Wang, *Science*, 2005, **310**, 1139–1143.
15 M. J. Bissell, H. G. Hall and G. Parry, *J. Theor. Biol.*, 2004, **99**(1), 31–68.
16 K. Jakab, C. Norotte, F. Marga, K. Murphy, G. Vunjak-Novakovic and G. Forgacs, *Biofabrication*, 2010, **2**, 022001.
17 S. Guven, P. Chen, F. Inci, S. Tasoglu, B. Erkmen and U. Demirci, *Trends Biotechnol.*, 2015, **33**(5), 269–279.
18 W. Sun, *et al.*, *Biofabrication*, 2020, **12**(2), 1–5.
19 C. S. O'Bryan, C. P. Kabb, B. S. Sumerlin and T. E. Angelini, *ACS Appl. Bio Mater.*, 2019, **2**, 1509–1517.
20 T. Bhattacharjee, C. P. Kabb, C. S. O'Bryan, J. M. Urueña, B. S. Sumerlin, W. G. Sawyer and T. E. Angelini, *Soft Matter*, 2018, **14**, 1559–1570.
21 T. Bhattacharjee, S. M. Zehnder, K. G. Rowe, S. Jain, R. M. Nixon, W. G. Sawyer and T. E. Angelini, *Sci. Adv.*, 2015, **1**(8), 1–6.
22 T. Bhattacharjee, C. J. Gil, S. L. Marshall, J. M. Urueña, C. S. O'Bryan, M. Carstens, B. Keselowsky, G. D. Palmer, S. Ghivizzani and C. P. Gibbs, *ACS Biomaterials Science & Engineering*, 2016, **2**, 1787–1795.

23 T. E. Angelini, A. C. Dunn, J. M. Urena, D. J. Dickrell, D. L. Burris and W. G. Sawyer, *Faraday Discuss.*, 2012, **156**, 31–39.
24 K. J. LeBlanc, S. R. Niemi, A. I. Bennett, K. L. Harris, K. D. Schulze, W. G. Sawyer, C. Taylor and T. E. Angelini, *ACS Biomater. Sci. Eng.*, 2016, **10**, 1796–1799.
25 S. Fukuda and G. W. Schmid-Schönbein, *Proc. Natl. Acad. Sci. U. S. A.*, 2003, **100**, 13152–13157.
26 R. Cohen, L. Amir-Zilberstein, M. Hersch, S. Woland, S. Taiber, F. Matsuzaki, S. Bergmann, K. B. Avraham and D. Sprinzak, *Nat. Commun.*, 2020, **11**, 5137.
27 D. A. Goodenough, *et al.*, *Cold Spring Harbor Perspect. Biol.*, 2009, **1**(1), 2576.
28 C. M. Nelson, M. M. Vanduijn, J. L. Inman, D. A. Fletcher and M. J. Bissell, *Science*, 2006, **314**, 298–300.
29 C. M. Nelson, *et al.*, *Proc. Natl. Acad. Sci. U. S. A.*, 2005, **102**, 11594–11599.
30 C. M. Nelson and M. J. Bissell, *Semin. Cancer Biol.*, 2005, **15**(5), 342–352.
31 J. V. Pagaduan, A. Bhatta, L. H. Romer and D. H. Garcias, *Small*, 2018, **14**, 1702497.
32 H. Yin, A. Varava and D. Kragic, *Sci Robot.*, 2021, **6**(54), DOI: **10.1126/scirobotics.abd8803**.
33 Y. Shen, D. A. Weitz, N. R. Forde and M. Shayegan, *Soft Matter*, 2022, **18**, 5359–5365.
34 S. C. Chapin, V. Germain and E. R. Dufresne, *Opt. Express*, 2006, **14**, 13095–13100.
35 S. Pradhan, C. P. Whitby, M. A. K. Williams, J. L. Y. Chen and E. Avci, *J. Colloid Interface Sci.*, 2022, **621**, 101–109.
36 K. Konig, *J. Microsc.*, 2001, **200**(2), 83–104.
37 N. Ji, *Nat. Methods*, 2017, **14**(4), 374–380.
38 V. Mironov, T. Boland, T. Trusk, G. Forgacs and R. Markwald, *Trends Biotechnol.*, 2003, **21**(4), 157–161.
39 A. Daly, M. Davidson and J. Burdick, *Nat. Commun.*, 2021, **12**(1), 753.
40 A. Blakely, K. Manning, A. Tripathi and J. Morgan, *Tissue Eng., Part C*, 2015, **21**(7), 737–746.
41 A. R. Lanza and E. C. Seaver, *Development*, 2020, **147**, 18.
42 B. Ayan, D. N. Heo, Z. Zhang, M. Dey and A. Povilianskas, *Sci. Adv.*, 2020, **6**(10), 13148.
43 B. Ayan, N. Celik, Z. Zhang, K. Zhou, M. H. Kim, D. Banerjee, Y. Wu, F. Costanzo and I. T. Ozbolat, *Commun. Phys.*, 2020, **3**(1), 1–14.
44 M. J. Layden, E. Röttinger, F. S. Wolenski, T. D. Gilmore and M. Q. Martindale, *Nat. Protoc.*, 2013, **8**(5), 924–934.
45 J. Candiello, *et al.*, *Biomaterials*, 2018, **177**, 27–29.
46 N. Tompkins, *et al.*, *Proc. Natl. Acad. Sci. U. S. A.*, 2014, **111**, 4397–4402.
47 A. Turing, *Philos. Trans. R. Soc., B*, 1953, **237**, 37–72.

